ELSEVIER

Computerized Medical Imaging and Graphics 29 (2005) 521–532

Computerized Medical Imaging and Graphics

www.elsevier.com/locate/compmedimag

# 3D localization of clustered microcalcifications using cranio-caudal and medio-lateral oblique views

Sheng-Chih Yang[a,b], Hsian-He Hsu[c], Giu-Cheng Hsu[c], Pau-Choo Chung[a], Shu-Mei Guo[d], Chien-Shen Lo[e], Ching-Wen Yang[f,*], San-Kan Lee[g], Chein-I Chang[h]

[a]*Department of Electrical Engineering, National Cheng Kung University Tainan, Taiwan 701, ROC*
[b]*Department of Electronic Engineering, National Chin Yi Institute of Technology Taichung, Taiwan 411, ROC*
[c]*Department of Radiology, Tri-Service General Hospital and National Defense Medical Center, Taipei, Taiwan 114, ROC*
[d]*Department of Computer Science and Information Engineering National Cheng Kung University, Tainan, Taiwan 701, ROC*
[e]*Department of Multimedia Design, National Formosa University, Yun-Lin, Taiwan 632, ROC*
[f]*Computer Center, Taichung Veterans General Hospital, Taichung, Taiwan 407, ROC*
[g]*Suao Veterans Hospital, Yilan County, Taiwan 270, ROC*
[h]*Remote Sensing Signal and Image Processing Laboratory, Department of Computer Science and Electrical Engineering, University of Maryland Baltimore County, Baltimore, MD 21250, USA*

Received 15 September 2004; revised 11 May 2005; accepted 11 May 2005

**Abstract**

This paper presents a 3D localization method to register clustered microcalcifications on mammograms from cranio-caudal (CC) and medio-lateral oblique (MLO) views. The method consists of three major components: registration of clustered microcalcifications in CC and MLO views, 3D localization of clustered microcalcifications and 3D visualization of clustered microcalcifications. The registration is performed based on three features, gradient, energy and local entropy codes that are independent of spatial locations of microcalcifications in two different views and are prioritized by discriminability in a binary decision tree. The 3D localization is determined by a sequence of coordinate corrections of calcified pixels using the breast nipple as a controlling point. Finally, the 3D visualization implements a virtual reality modeling language viewer (VRMLV) to view the exact location of the lesion as a guide for needle biopsy. In order to validate our proposed 3D localization system, a set of breast lesions, which appear both in mammograms and in MR Images is used for experiments where the depth of clustered microcalcifications can be verified by the MR images.


*Keywords:* 3D localization; Cranio-caudal (CC) view; Mammogram; Medio-lateral oblique (MLO) view; Microcalcifications

## 1. Introduction

Breast lesions always require the results of cytology or pathology examination to make a decision for further management. For non-palpable breast lesions, especially mammography detectable microcalcifications, the locations of lesions can be only identified from two views on mammograms, the cranio-caudal (CC) view and medio-lateral oblique (MLO) view. However, it is often the case that when there are multiple clusters of microcalcification, or the image quality is poor, it is generally difficult to localize such clustered microcalcifications by these two views. In this case, we may have to use wire localization to identify their presence. With this procedure, additional manpower and preparation will be needed. This may also include an increase of X-ray dose and extra exposures for needle localization. It is not only hazardous to patients, but also may waste medical resources.

Unfortunately, computing 3D positions for breast lesions on mammograms has received little attention due to the fact that breast compression involves a complicated relationship between the 2D positions resulting from two different views (CC and MLO views) and its actual 3D position in the uncompressed breast. Recently, Niklason et al. [1] combined multiple views of a breast to reconstruct the 3D

* Corresponding author. Tel.: +42 3741 211; fax: +42 3590 506.
*E-mail address:* cwyang@vghtc.gov.tw (C.-S. Lo).

0895-6111/$ - see front matter © 2005 Elsevier Ltd. All rights reserved.
doi:10.1016/j.compmedimag.2005.05.001

information of the breast based on tomosynthesis to help the radiologists locate the microcalcifications and tumors in the breast in a 3D position. Maidment et al. [2] also proposed another approach based on a stereo breast biopsy system from seven views. To remove the requirement of multiple views, Chang et al. [3] compared two computerized methods, the arc and Cartesian straight-line, for the localization of breast lesion in two mammographic views. Cho et al. [4] simply used Cartesian coordinate and computer graphics of the two views to compute the localization of breast lesions without adjustment of compression. Yam et al. [5] presented a novel model-based method for reconstructing microcalcifications of a breast by incorporating with a prior geometric model from two mammograms, and used a number of tissue movement approximations to adjust the compressed breast. Although their method did not need multiple mammograms, there was a limitation of requiring a general breast model to assist back projection of the microcalcifications toward the X-ray source. Kita et al. [6] calculated curved epipolar lines by simulating breast deformation into stereo camera geometry to estimate the 3D location of a lesion, but the issue of registration between two views was not discussed.

In this paper, we develop a computer-aided three-dimensional (3D) localization system for viewing microcalcifications. It takes the CC and MLO views of mammograms as an input to reconstruct a 3D breast model that can pinpoint the precise locations of microcalcifications. This model can reduce number of needle punctures for biopsy preoperatively, and provide breast surgeons with the location of lesions during the operation. The hardware of the proposed system includes an equipment to obtain the digital images of X-ray mammography and networking to a personal computer (PC) which is also used as an output to show the 3D figure of breast for visualization. Our developed software consists of several custom-designed image processing techniques, which are (1) feature extraction from one view, (2) auto-detection and registration of the clustered microcalcifications in the other view, (3) auto-detection of the nipple, and (4) adjustment of clustered microcalcifications on both CC and MLO views in order to visualize the location and distribution of clustered microcalcifications accurately.

In order to validate our proposed system, phantom experiments are first used to substantiate the software, then followed by real image experiments which are conducted by taking MR images and two views of mammograms from the same patient at the same time. Since MR images do not require compression of breasts, they can provide precise locations of microcalcifications and can be used to verify the 3D localization viewed by VRMLV. Such MRI/mammogram experiments further verify the utility of our system in medical and clinical applications for 3D localization and visualization of microcalcifications.

## 2. Registration of clustered microcalcifications in CC and MLO views

Detection of microcalcifications has been studied extensively over the past years. Most of cases are based on a single view, either CC or MLO view. It is of interest to see if the information of microcalcifications detected in these two different views can be fused and integrated so as to improve medical diagnosis and clinical applications. One of major obstacles is how to register clustered microcalcifications on mammograms from the CC and MLO views.

The need of registration of clustered microcalcifications arises from the fact that microcalcifications shown in the CC view may not be seen in the MLO view, or vice versa. In addition, a group of clustered microcalcifications in one view may be separated into several groups of clustered microcalcifications in another view. In order to resolve this issue, we need to find features that specify mammographic characteristics of clustered microcalcifications, but are independent of their spatial locations from different views. In what follows, three features are developed for this purpose and described in detail.

### 2.1. Three features used for experiments

As mentioned previously, the features used for 3D localization must be independent of CC and MLO views. In order to accomplish this goal, three types of features are proposed in this section to fuse clustered microcalcifications from the two views for 3D localization, which are gradient code (GC), energy code (EC) and local entropy code (LEC). The GC captures changes in gray levels of each of clustered microcalcifications. The EC describes the energy of each of clustered microcalcifications in terms of variance. LEC measures the information contained in each of clustered microcalcifications.

#### 2.1.1. Gradient code (GC)

The gradient code (GC) is calculated based on so-called spatial gray scale co-occurrence matrix (SGLCM) commonly used in texture analysis [7,8]. It is a matrix that keeps track of changes in transition between two gray levels. More specifically, assume that the gray level range is $G=\{0,1,\ldots,L-1\}$. Let $n_{ij}$ be the number of transitions made from gray level $i$ to gray level $j$ according to two pixel relative locations. In this paper, $n_{ij}$ is defined by

$$n_{ij} = \sum_{l=1}^{M}\sum_{k=1}^{N}\delta(l,k) \tag{1}$$

where

$$\delta(l,k) = \begin{cases} 1; & \text{if}(I(l,k)=i \text{and} I(l,k-1)=j) \\ & \quad \text{or}(I(l,k)=i \text{and} I(l-1,k)=j) \\ 0; & \text{otherwise} \end{cases} \tag{2}$$

and $I(l,k)$ is the gray level of the pixel at location $(l,k)$ and $M\times N$ is the size of the image. From Eq. (1) we further define $n=\sum_{i=0}^{L-1}\sum_{j=0}^{L-1} n_{ij}$ with indices $i$ and $j$ over the gray level range $G$. In this case, we can calculate the transition probability from gray level $i$ to gray level $j$ by $p_{ij}=n_{ij}/n$. By virtue of $\{p_{ij}\}_{i=0,j=0}^{L-1,L-1}$ the SGLCM is defined by $\mathbf{W}=[p_{ij}]_{i,j\in G}$. Let $\tau$ be an arbitrary gray level in $G$ and partitions the gray level range $G$ into the two regions $G_0=\{0,1,\ldots,\tau\}$ and $G_1=\{\tau+1,\ldots,L-1\}$. By means of the threshold $\tau$ the SGLCM can be further partitioned into four quadrants, BB, BF, FB and FF with their gray level regions specified by $G_0\times G_0$, $G_0\times G_1$, $G_1\times G_0$ and $G_1\times G_1$, respectively, as shown in Fig. 1. Since objects usually appear in the foreground and can be segmented by FF, we define the GC via FF by

$$\mathrm{GC}=\frac{1}{(L-\tau)(L-\tau)}\sum_{i=\tau+1}^{L-1}\sum_{j=\tau+1}^{L-1}|i-j|p_{ij}. \tag{3}$$

#### 2.1.2. Energy code (EC)

In order to define energy code (EC), we divide a mammogram into $64\times64$ image blocks. For each given $64\times64$ image block, we further define a vector $\mathbf{x}_i=(x_{i1},x_{i2},\ldots,x_{i64})^T$ formed by all the 64 pixels in the $i$-th row in the image block. The correlation matrix of this particular image block can be calculated by $\mathbf{R}=\frac{1}{64}\sum_{i=1}^{64}\mathbf{x}_i\mathbf{x}_i^T$. The EC is then defined by the largest eigenvalue of $R$. To be precise, if $\{\lambda_i\}_{i=1}^{64}$ are the eigenvalues of $R$, the EC is defined by $\mathrm{EC}=\lambda_{\max}=\max_{1\le i\le 64}\{\lambda_i\}$.

#### 2.1.3. Local entropy code (LEC)

Entropy is widely used in information theory [7–9] to measure the information content in a source. If we consider the objects segmented by FF as an information source, we can use its entropy to describe how much information contained in these objects. In doing so, we need to normalize the transition probabilities in the quadrant FF to unity by

$$p_{ij}^{FF}=\frac{n_{ij}}{\sum_{i=\tau+1}^{L-1}\sum_{j=\tau+1}^{L-1}n_{ij}}=\frac{n_{ij}/n}{\left(\sum_{i=\tau+1}^{L-1}\sum_{j=\tau+1}^{L-1}n_{ij}/n\right)}=\frac{p_{ij}}{\sum_{i=\tau+1}^{L-1}\sum_{j=\tau+1}^{L-1}p_{ij}}. \tag{4}$$

From Eq. (4) $\{p_{ij}^{FF}\}_{i\in G_1,j\in G_1}$ forms a probability distribution of the FF and its corresponding entropy can be calculated by

$$H_{FF}(\tau)=-\sum_{i=\tau+1}^{L-1}\sum_{j=\tau+1}^{L-1}p_{ij}^{FF}\log p_{ij}^{FF} \tag{5}$$

The local entropy code (LEC) is then defined by Eq. (5), i.e. $\mathrm{LEC}=H_{FF}(\tau^*)$ where $\tau^*$ is an optimal threshold that can be determined by the local entropy method in [7].

### 2.2. Registration procedure

First of all, we assume that clustered microcalcifications in the CC and MLO views are objects of interest which can be considered as the foreground, while the rest of the image is background. In this subsection, we propose a method to register clsutered microcalcifications in both views. It is a hierarchical process shown in Fig. 2 which uses a binary tree to prioritize the three features, GC, EC and LEC in order. This priority order is an empirical selection resulting from our experiments.

#### 2.2.1. Registration procedure:

1. Divide images in the mammograms from CC and MLO views into $64\times64$ image blocks with half block (i.e. $32\times32$) overlapped.
2. For each image block, calculate GC, EC and LEC.
3. All the image blocks in the mammograms from the CC view and MLO view are prioritized in the order of GC, EC and LEC using a binary decision tree.
4. When the decision reaches to a tree leaf, each image block in the mammograms from both CC and MLO views is prioritized according to the three features GC,

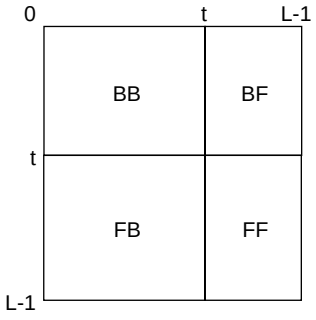


Fig. 1. SGLCM partitioned into BB, BF, FB, FF regions.

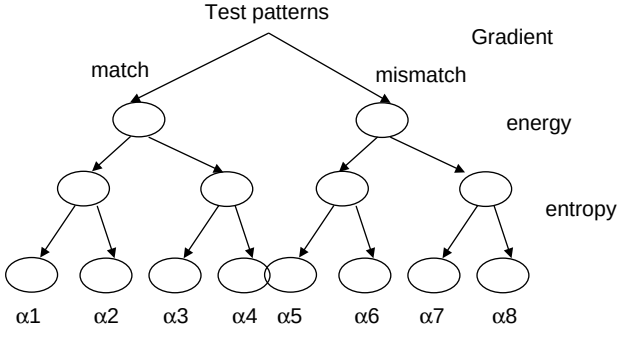


Fig. 2. A flow chart of a binary decision tree prioritizing the registration features.

EC and LEC. For example, according to the priority order used in Fig. 2 a left offspring means a match, while a right one indicates a mismatch. There are three levels in the tree. The top level is first prioritized by the GC, followed by the second and third levels measured by the EC and the LEC, respectively. There are eight tree leaves, denoted by $\alpha_1$ to $\alpha_8$ representing eight different priorities resulting from the three features. The tree leave $\alpha_1$ denotes that all the three features are matched compared to the tree leave $\alpha_8$ with no feature matched at all. The tree leaves between $\alpha_1$ and $\alpha_8$ represent different levels of matching using the three features.

## 3. 3D localization of clustered microcalcifications

In Section 2, we developed a method to register clustered microcalcifications from both CC and MLO views. Next step is to compute the spatial locations of (CC view, MLO view)-registered clustered microcalcifications in 3D coordinates.

### *3.1. Coordinate correction using nipple's position as a controlling point*

First of all, a controlling point for both views is required for coordinate correction. A natural choice is the nipple of a breast. In this case, we need to first register the coordinate of the nipple in both CC and MLO views. This can be done by either manually or an automatic localization method proposed by Chandrasekhar et al. [10]. After the nipple is registered, we can adjust the nipple in such a manner that it is located at origin of a 3D coordinate system. Let ($x_{\text{nipple,CC}}$, $z_{\text{nipple,CC}}$) and ($y_{\text{nipple,MLO}}$, $z_{\text{nipple,MLO}}$) be its spatial coordinates in the CC and MLO views, respectively. Using the nipple as a 3D point coordinate, any point ($x_{\text{CC}}$,$z_{\text{CC}}$) in the CC view can be further adjusted by $(\tilde{x}_{\text{CC}}, \tilde{z}_{\text{CC}}) = (x_{\text{CC}} - x_{\text{nipple,CC}}, z_{\text{CC}} - z_{\text{nipple,CC}})$. Similarly, for any point ($y_{\text{MLO}}$, $Z_{\text{MLO}}$) in MLO view, it can be also adjusted by $(\tilde{y}_{\text{MLO}}, \tilde{z}_{\text{MLO}}) = (y_{\text{MLO}} - y_{\text{nipple,MLO}}, z_{\text{MLO}} - z_{\text{nipple,MLO}})$. Since the MLO view is oblique, the coordinates ($\tilde{y}_{\text{MLO}}$, $\tilde{z}_{\text{MLO}}$) can be further corrected by including a rotation angle ($\tilde{y}_{\text{MLO}} \cos\theta, \tilde{z}_{\text{MLO}} \cos\theta$). However, for an illustrative purpose, we assume $\theta = 90°$ without loss of generality, i.e. the MLO view is perpendicular to CC view.

### *3.2. 3D representations of clustered microcalcifications for CC and MLO views*

The CC and MLO views only show 2D images. For the purpose of clarity we assume that the CC and MLO views are represented by $X-Z$ plane and $Y-Z$ plane as shown in Fig. 3(a) and (b), respectively.

Suppose that $\zeta = (x,y,z)$ is the point to visualize a point ($x_{\text{CC}}$,$z_{\text{CC}}$) in the CC view and a point ($y_{\text{MLO}}$, $z_{\text{MLO}}$) in the MLO view in a 3D space. After the nipple has been determined and fixed at the origin as described in Section 3.1, ($x_{\text{CC}}$, $z_{\text{CC}}$) in the CC view and ($y_{\text{MLO}}$, $z_{\text{MLO}}$) in the MLO view are then adjusted to be ($\tilde{x}_{\text{CC}}$, $\tilde{z}_{\text{CC}}$) and ($\tilde{y}_{\text{MLO}}$, $\tilde{z}_{\text{MLO}}$), respectively. Correspondingly, $\zeta = (x,y,z)$ is also adjusted in the same way as was done for $\tilde{\zeta} = (\tilde{x}, \tilde{y}, \tilde{z})$. In order to find the 3D spatial coordinates of $\tilde{\zeta} = (\tilde{x}, \tilde{y}, \tilde{z})$, we need an auxiliary coordinate $\tilde{y}_{\text{CC}}$ for ($\tilde{x}_{\text{CC}}$, $\tilde{z}_{\text{CC}}$) in the CC view and another auxiliary coordinate $\tilde{x}_{\text{MLO}}$ for ($\tilde{y}_{\text{MLO}}$, $\tilde{z}_{\text{MLO}}$) in the MLO view to represent both views in a 3D visualization space. Let ($\tilde{x}_{\text{CC}}, \tilde{y}_{\text{CC}}, \tilde{z}_{\text{CC}}$) and ($\tilde{x}_{\text{MLO}}, \tilde{y}_{\text{MLO}}, \tilde{z}_{\text{MLO}}$) be their 3D corresponding coordinates. Since both the CC and MLO views share the common coordinate, $z$-axis, we can use it as a base and calculate their relative positions. A simple way is to assume that the point $\tilde{\zeta} = (\tilde{x}, \tilde{y}, \tilde{z})$ is the midpoint between ($\tilde{x}_{\text{CC}}, \tilde{y}_{\text{CC}}, \tilde{z}_{\text{CC}}$) and ($\tilde{x}_{\text{MLO}}, \tilde{y}_{\text{MLO}}, \tilde{z}_{\text{MLO}}$). More precisely, we use the following equation

$$\frac{\tilde{x}_{\text{CC}}}{\tilde{x}_{\text{MLO}}} = \frac{\tilde{y}_{\text{CC}}}{\tilde{y}_{\text{MLO}}} = \frac{\tilde{z}_{\text{CC}}}{\tilde{z}_{\text{MLO}}} \tag{6}$$

to generate the two auxiliary coordinates, $\tilde{y}_{\text{CC}}$ and $\tilde{x}_{\text{MLO}}$ given by

$$\tilde{y}_{\text{CC}} = \left(\frac{\tilde{z}_{\text{CC}}}{\tilde{z}_{\text{MLO}}}\right) y_{\text{MLO}} \quad \text{and} \quad \tilde{x}_{\text{MLO}} = \left(\frac{\tilde{z}_{\text{MLO}}}{\tilde{z}_{\text{CC}}}\right) \tilde{x}_{\text{CC}}. \tag{7}$$

From Eqs. (6) and (7), the desired point $\tilde{\zeta} = (\tilde{x}, \tilde{y}, \tilde{z})$ for 3D localization of the point ($\tilde{x}_{\text{CC}}, \tilde{y}_{\text{CC}}, \tilde{z}_{\text{CC}}$) in the CC view

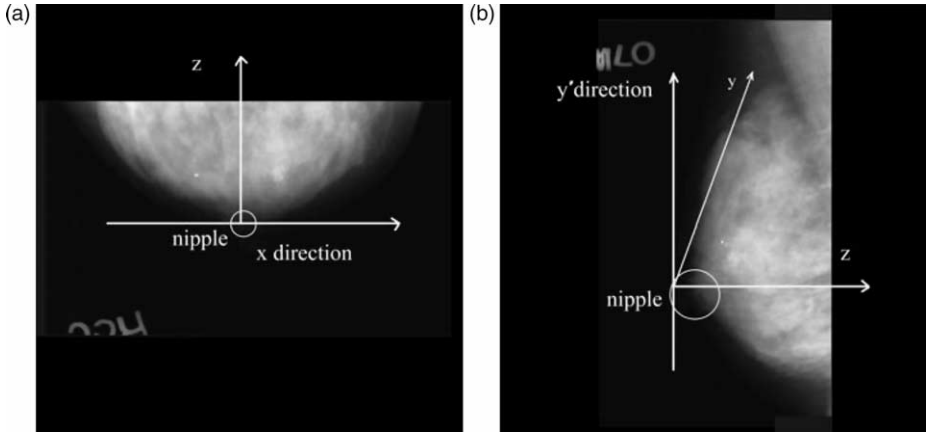


Fig. 3. (a) A CC view represented by X–Z plane. (b) An MLO view represented by Y–Z plane.

and $(\tilde{x}_{MLO}, \tilde{y}_{MLO}, \tilde{z}_{MLO})$ in the MLO view can be further determined by

$$\tilde{x} = \frac{\tilde{x}_{MLO} + \tilde{x}_{CC}}{2}, \quad \tilde{y} = \frac{\tilde{y}_{MLO} + \tilde{y}_{CC}}{2}, \quad \tilde{z} = \frac{\tilde{z}_{MLO} + \tilde{z}_{CC}}{2}. \tag{8}$$

So, for any point $\zeta = (x,y,z)$ corresponding to the point $(x_{CC}, z_{CC})$ in the CC view and the point $(y_{MLO}, z_{MLO})$ in MLO view, its 3D spatial coordinate can be obtained by Eq. (8) as $\tilde{\zeta} = (\tilde{x}, \tilde{y}, \tilde{z})$.

## 4. Coordinate correction resulting from breast compression

Due to the fact that the mammograms in the CC and MLO views are obtained by compressing breasts, the coordinates of clustered microcalcifications in both views will be quite different. As a result, the calculation for the coordinates of 3D localization of clustered microcalcifications proposed in Section 3 may not be accurate. In this case, the bias caused by breast compression must be estimated for correction. This section presents such methods that can accurately calculate the 3D spatial coordinates of clustered microcalcifications in uncompressed breasts via their appearance in the CC and MLO views. In what follows, a cluster of microcalcifications will be referred to as a region of interest (ROI).

First of all, four assumptions must be made.

1. The volume of a breast is compression-invariant. That is, the volume of a breast remains unchanged after a breast is compressed.
2. The shape of a breast can be modeled by a hemisphere as shown in Fig. 4.
3. The shape of a compressed breast can be modeled by a semi-cylinder as shown in Fig. 5.

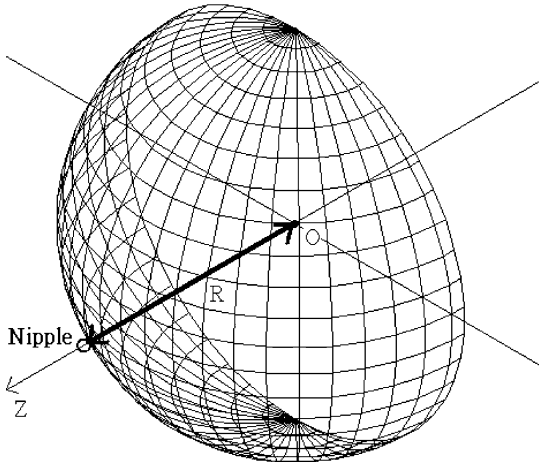


Fig. 4. Hemisphere model for an uncompressed breast.

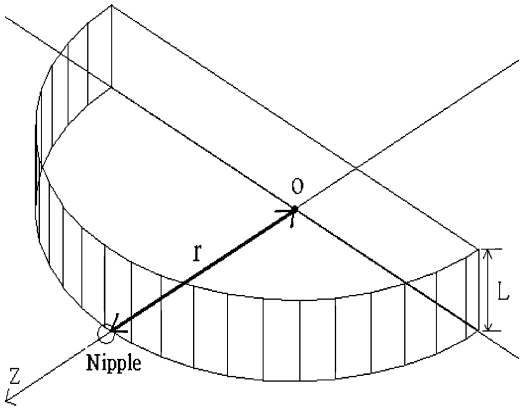


Fig. 5. Semi-cylinder model for a compressed breast.

4. The nipple of a breast must be on the breast surface and located at the $z$-axis.

Based on the above assumptions, we can calculate the volume of a hemisphere by

$$\frac{1}{2}\frac{4\pi R^3}{3} \tag{9}$$

where $R$ is the radius of the hemisphere and the volume of a semi-cylinder by

$$\frac{1}{2}\pi r^2 L \tag{10}$$

where $r$ and $L$ is the radius and height of the semi-cylinder, respectively. Due to volume invariance under breast compression (i.e. assumption 1), Eq. (9) must be equal to Eq. (10), that is

$$\frac{1}{2}\frac{4\pi R^3}{3} = \frac{1}{2}\pi r^2 L \Rightarrow R^3 = \frac{3r^2 L}{4} \tag{11}$$

which implies that the radius $R$ of an uncompressed breast can be solved by the radius $r$ and height $L$ (i.e. thickness) of a compressed breast via Eq. (11).

Since our proposed 3D localization system is based on two views (CC and MLO) which do not provide the depth information, the parameter specified by $L$ is included for this purpose to estimate the thickness that reflects the breast depth. In doing so, we have taken advantage of an advanced digital mammography instrument available in the TaiChung Verterans General Hospital (TCVGH) to collect a large sample pool that can provide actual measurements of the two parameters $r$ and $L$ to validate this parameter $L$. Two approaches can be used to estimate the parameter $L$. One is a sample average method which categorizes samples in accordance with the radius $r$ in the ranges of 55–60, 60–65,…,100–105 mm with 5 mm apart. For each category, we calculated the averaged value of $L$ and the error resulting from the difference between the obtained averaged $L$ and the real $L$ value of samples. It was shown empirically that the error for each category ranged from 0.26 to 20.6 mm with averaged error of 6.76 mm.

A second method is to derive a linear equation that can describe the correlation between $r$ and $L$ in the sense of least squares error (LSE). Assume that a linear equation is modeled by

$$L = c_1 + c_2 r \tag{12}$$

where $c_1$ and $c_2$ are unknown constants and yet to be determined. If the LSE criterion is used as a criterion for goodness of fit, the $c_1$ and $c_2$ can be derived from a set of sample data $\{(r_i, L_i)\}_{i=1}^{N}$ as follows

$$c_1 = \frac{\begin{vmatrix} \sum_{i=1}^{N} r_i & \sum_{i=1}^{N} r_i \\ \sum_{i=1}^{N} r_i & \sum_{i=1}^{N} x_i^2 \end{vmatrix}}{\begin{vmatrix} N & \sum_{i=1}^{N} r_i \\ \sum_{i=1}^{N} r_i & \sum_{i=1}^{N} r_i^2 \end{vmatrix}} \quad \text{and}$$

$$c_2 = \frac{\begin{vmatrix} N & \sum_{i=1}^{N} L_i \\ \sum_{i=1}^{N} r_i & \sum_{i=1}^{N} r_i L_i \end{vmatrix}}{\begin{vmatrix} N & \sum_{i=1}^{N} r_i \\ \sum_{i=1}^{N} r_i & \sum_{i=1}^{N} r_i^2 \end{vmatrix}}. \tag{13}$$

Following similar experiments to those conducted for the sample average method, the LSE-based method produced errors for different categories ranging from 0.13 to 17.79 mm with the averaged error of 6.62 mm which was slightly better than 6.76 mm produced by the sample average method. Therefore, the LSE-based method was used to estimate the parameter in our paper.

In order to solve $c_1$ and $c_2$ in Eq. (13), 118 cases were collected in the TCVGH and used as the sample data with the solution obtained by $c_1 = 0.32049$ and $c_2 = 0.50385$. Substituting the obtained $c_1$ and $c_2$ into Eq. (12), the $r$ and $L$ can be linearly correlated by the following equation

$$L = 0.32049 + 0.50385r. \tag{14}$$

By means of Eqs. (11) and (14), the radius of an uncompressed breast, $R$ can be solved by

$$R^3 = \frac{3r^2(0.32049 + 0.50385r)}{4} \tag{15}$$

Now based on Eq. (15) two correction methods can be developed to correct the bias caused by the 3D localization method proposed in Section 3.

A comment is noteworthy. Due to advances of digital mammography which can provide actual measurements of compressed breast in two different views, it may eventually not need to estimate depth at all in the future. In this case, our developed system can be further improved by its accuracy in 3D localization.

### 4.1. Method 1

Since an ROI (i.e. a cluster of microcalcifications) is always inside the breast, we can consider another semi-cylinder (i.e. the thickness of the compressed breast on a mammogram) with the ROI on the surface and its radius, denoted by $r'$ measured from the ROI to the chest wall of the compressed breast as shown in Fig. 6 where the origin O is the same one in Figs. 4 and 5.

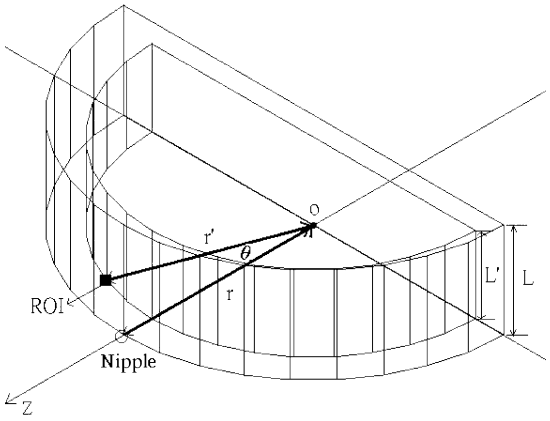


Fig. 6. Spatial coordinates of an ROI within a compressed breast.

Firstly, we can measure the radius r from the nipple to the chest wall of the compressed breast in the mammogram and use Eq. (15) to calculate a correct estimate of the radius $R$ shown on Fig. 7. According to our method, the nipple is located at the $z$-axis. Therefore, as illustrated in Fig. 6, the polar coordinate of the nipple of uncompressed breast can be obtained.

In order to estimate the radius $R'$ which is measured from an ROI to the chest wall of an uncompressed breast, we first let $L'$ denote the height of the semi-cylinder where the ROI is assumed on its surface. Then the $L'$ can be found via the following equation

$$\frac{r}{r'} = \frac{L}{L'}. \tag{16}$$

As illustrated in Fig. 7, the $R'$ can be calculated by substituting the $L'$ obtained by Eq. (16) into Eq. (15). We can further measure the angle $\theta$ from the mammogram in Fig. 7 and the polar coordinates of the ROI of uncompressed breast as $(R',\theta)$. Once the polar coordinates of the nipple and the ROI in the uncompressed breast are determined, we can

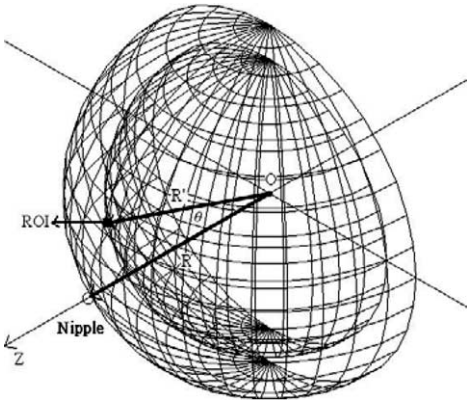


Fig. 7. Spatial coordinates of an ROI within an uncompressed breast.

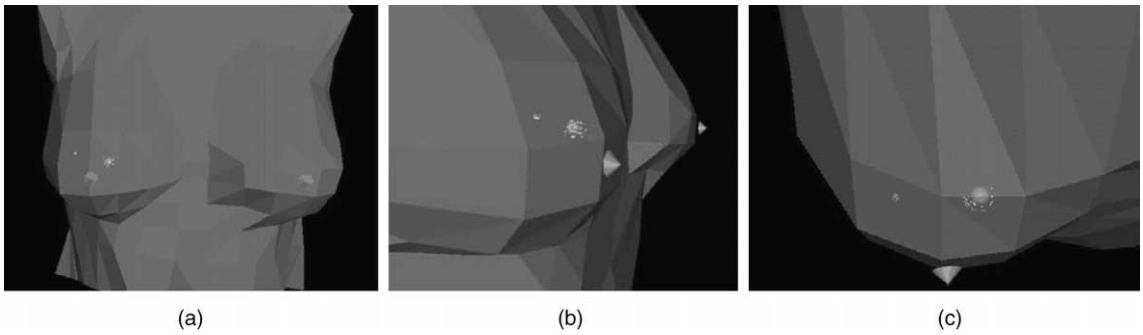


Fig. 8. (a) One view of 3D visualization of two groups of clustered microcalcifications. (b) An oblique view of 3D visualization. (c) A cranio-caudal view of 3D visualization.

further correct the spatial coordinates of $(\tilde{x}_{CC}, \tilde{z}_{CC})$ and $(\tilde{y}_{MLO}, \tilde{z}_{MLO})$ which corresponds to the ROI in an uncompressed breast as the nipple located at the origin. Finally, the spatial coordinates of the 3D localization of the ROI within an uncompressed breast can be obtained via Eqs. (6)–(8).

### 4.2. Method 2

Another method which is more simpler than Method 1 is to measure the radius $r$ of the ROI from the chest wall of a compressed breast on the mammogram, then further to calculate the radius $R$ of the ROI from an uncompressed breast via Eq. (15). Using the ratio of $R$ to $r$, $R/r$ allows us to correct the spatial coordinates of $(\tilde{x}_{CC}, \tilde{z}_{CC})$ and $(\tilde{y}_{MLO}, \tilde{z}_{MLO})$ in an uncompressed breast by the following equation

$$(\tilde{x}_{CC}, \tilde{z}_{CC}) = (\tilde{x}_{CC}R/r, \tilde{z}_{CC}R/r) \quad \text{and}$$
$$(\tilde{y}_{MLO}, \tilde{z}_{MLO}) = (\tilde{y}_{MLO}R/r, \tilde{z}_{MLO}R/r). \tag{17}$$

Finally, the spatial coordinates of the 3D localization of the ROI within an uncompressed breast can be obtained via Eqs. (6)–(8).

## 5. Visualization of clustered microcalcifications

Once the spatial locations of the registered clustered microcalcifications are obtained, we will represent the registered clustered microcalcifications in a 3D visualization breast model. Although a point $\zeta = (x,y,z)$ in clustered microcalcifications has been corrected by $\tilde{\zeta} = (\tilde{x}, \tilde{y}, \tilde{z})$ via Eq. (8), its coordinates may vary with the size of the breast. For the sake of visualization, the model used to display clustered microcalcifications in a 3D visualization space should not be affected by the breast size. In this case, we need a standardized 3D breast model for visualization. This can be accomplished by normalizing a breast to a standard size. In doing so, let $D_{CC}$ and $D_{MLO}$ be the depth of a breast in the CC and MLO views, respectively, where the breast depth is measured by the shortest distance from the nipple to the breast chest wall. If we further let $D = (D_{CC} + D_{MLO})/2$, we can find new 3D coordinates of $\tilde{\zeta} = (\tilde{x}, \tilde{y}, \tilde{z})$ given by Eq. (8) in our standardized 3D breast model by $\zeta^* = (x^*,y^*,z^*)$ using the following equation

$$x^* = \frac{\tilde{x}}{D}, \quad y^* = \frac{\tilde{y}}{D}, \quad z^* = \frac{\tilde{z}}{D}. \tag{18}$$

Fig. 8(a) shows a 3D visualization version of two groups of registered clustered microcalcifications in a 3D standard breast model resulting from a 3D MLO view and a 3D CC view in Fig. 8(b) and (c) where the two bright spots on the right breast are the areas of two groups of clustered microcalcifications.

## 6. Experiments

Two sets of experiments were designed to validate the 3D localization system proposed in this paper along with two methods used for bias correction. The first set of experiments was conducted based on breast phantom images which were used for proof-of-concept. The second set of experiments used real images to justify the utility of our proposed system in clinical applications.

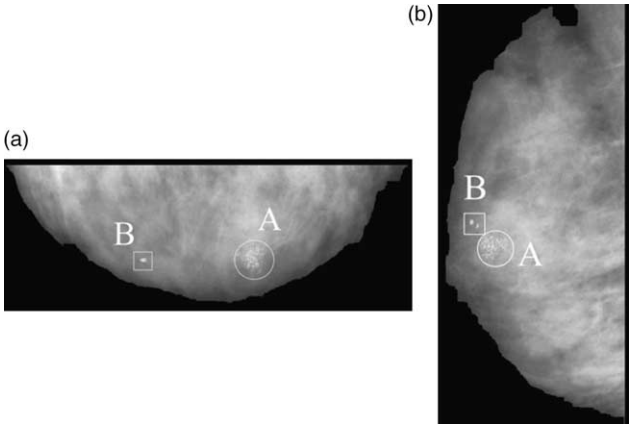


Fig. 9. Mammograms used for 3D localization test. (a) A CC view. (b) An MLO view.

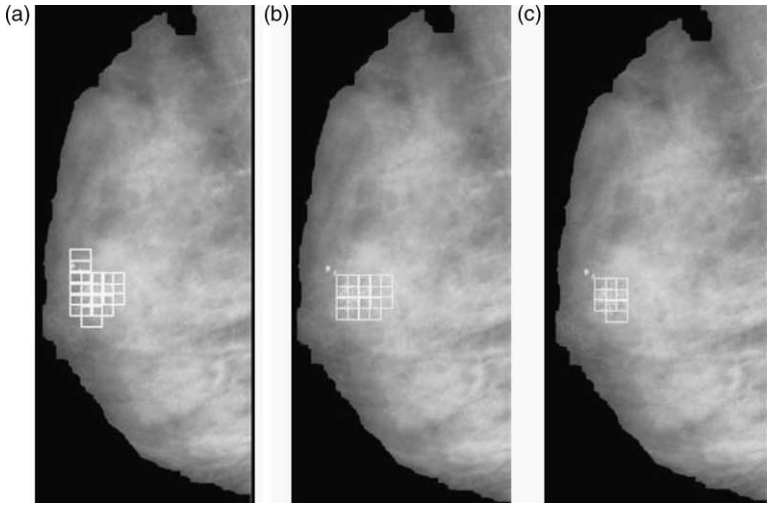


Fig. 10. Registered image blocks of the case of Fig. 5. (a) Image resulting from using GC as the first registration feature. (b) Image resulting from of Fig. 6(a) using EC as the second registration feature. (c) Image resulting from of Fig. 6(b) using LEC as the third registration feature.

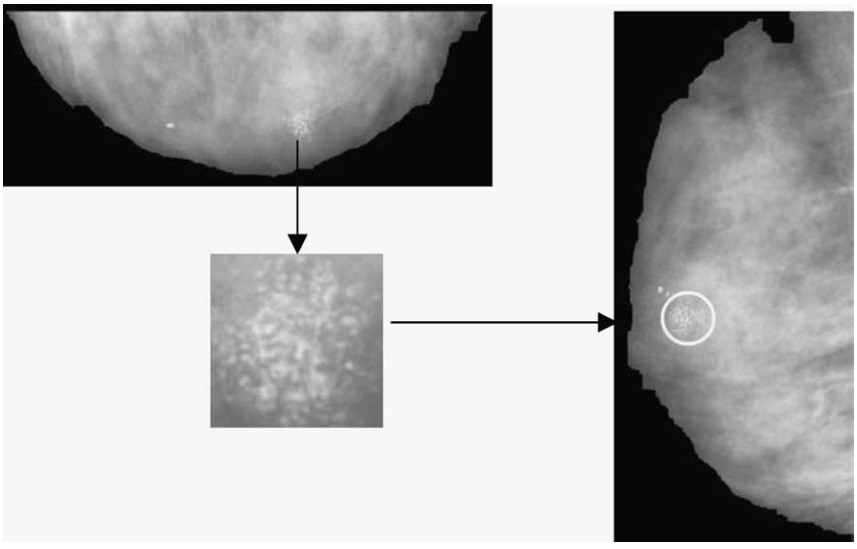

Fig. 11. Final result of registering Fig. 9(a) and (b).

### 6.1. Registration of CC and MLO views

In this section, 10 pairs of mammograms from the CC and MLO views were used to evaluate the proposed 3D localization system for registration. Among them were three cases with two groups of clustered microcalcifications and the other seven cases with only one group of clustered microcalcifications. So, a total of 13 groups of clustered microcalcifications was used for experiments.

Fig. 9(a) and (b) shows an example of our experiments using mammograms from the CC and MLO views where two groups of clustered microcalcifications are marked by a circle with A and a rectangle with B. Clearly, group A and group B are well-separated in Fig. 9(a) but not in Fig. 9(b). In this example, we used the CC view to register the MLO view since it was more difficult to use the MLO view to register the CC view. Fig. 10(a)–(c) shows registered image block patterns using GC, EC and LEC as priority features in accordance with the flow chart in Fig. 2. Fig. 10(a) is the result of using GC as the first registration feature. The purpose of using GC was to detect changes in gray levels of

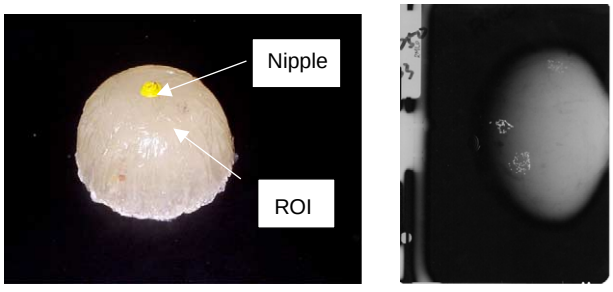


Fig. 12. (a) Silicon-made phantom (b) X-rayed phantom.

Table 1
True and calculated coordinates of ROI in phantom cases

| Case no. | True coordinate (mm) | Calculated coordinate with no bias correction (mm) | Calculated coordinate with bias correction by Method 1 (mm) | Calculated coordinate with bias correction by Method 2 (mm) |
|---|---|---|---|---|
| 1 | (−40,42,43) | (−53.07,64.51,69.25) | (−42.97,50.6,53.47) | (−43.41,51.94,55.49) |
| 2 | (−9,13,23) | (−10.09,14.37,27.25) | (−8.5,11.59,20.48) | (−7.55,10.75,20.37) |
| 3 | (17,−16,31) | (21.96,−16.8,42) | (16.39,−12.61,31.51) | (16.42,−12.55,31.39) |
| 4 | (8,−12,46) | (15.1,−13.41,74.5) | (10.68,−10.08,56.28) | (11.39,−10.11,56.17) |
| 5 | (−15,7,12) | (−13,14,18) | (−9.66,9.93,13.55) | (−9.81,10.56,13.57) |
| 6 | (29,−25,37) | (49.−48,46) | (38.02,−36.63,34.7) | (36.94,−36.19,34.68) |

Table 2
Euclidean distance (ED) between true and calculated coordinates of ROI in phantom cases

| Case no. | ED between true and calculated coordinate (with no bias correction) (mm) | ED between true and calculated coordinate (with bias correction by Method 1) (mm) | ED between true and calculated coordinate (with bias correction by Method 2) (mm) |
|---|---|---|---|
| 1 | 36.97 | 13.87 | 16.32 |
| 2 | 4.6 | 2.93 | 4.24 |
| 3 | 12.1 | 3.48 | 3.52 |
| 4 | 29.4 | 10.8 | 10.89 |
| 5 | 9.43 | 6.29 | 6.49 |
| 6 | 31.78 | 14.9 | 13.92 |

groups of clustered microcalcifications to make sure that none of clustered microcalcifications will be missed during registration. As shown in Fig. 10(a), A and B were first extracted for registration, then were separated in Fig. 10(b) using EC as the second registration feature for Fig. 10(a). Fig. 10(c) was produced by using the third registration feature LEC for Fig. 10(b). Since the image in Fig. 10(c) was obtained by registration of image block patterns from the CC and MLO views, the diameters of the two groups of registered clustered microcalcifications were recalculated. Fig. 11 is the final result of registering Fig. 9(a) and (b). Using Fig. 11 as a guide the two groups of clustered microcalcifications were localized in a 3D visualization space shown in Fig. 8(a)–(c) via a 3D breast model.

The results showed that our proposed registration method of registering these 13 groups of clustered microcalcifications could achieve the accuracy as high as 98%.

### 6.2. Validation of 3D localization

In order to validate our proposed 3D localization system with bias correction, experiments using phantoms and magnetic resonance (MR) images were conducted for performance evaluation.

#### 6.2.1. Phantom experiments

The breast phantom used for our experiments was made by silicon as shown in Fig. 12(a) and the nipple was identified by a spiraled wire. The clustered microcalcifications were made by iron filings and implanted in the breast phantom as shown in Fig. 12(b). Since the silicon is transparent, we can visually see the clustered microcalcifications through the breast phantom. Therefore, the coordinates of the clustered microcalcifications can be easily measured by visual inspection. Table 1 tabulates the true and calculated coordinates of the clustered microcalcifications via the 3D localization calculation described in Section 3 with no bias correction and with bias correction by Method 1 and Method 2 described in Section 4. In order to see how close between the true and calculated coordinates is, Table 2 computes the Euclidean distance between true and calculated coordinates and tabulates the errors where the errors corrected by two methods were much smaller than those obtained by direct 3D localization calculation with no bias correction. Additionally, Method 1 seemed to yield smaller errors than did Method 2. Nevertheless, Method 2 has an advantage over Method 1 in terms of simplicity. The phantom experiments demonstrated that our 3D localization system was effective.

Table 3
True and calculated coordinates of ROI in MRI cases

| Case no. | True coordinate (mm) | Calculated coordinate with no bias correction (mm) | Calculated coordinate with bias correction by Method 1 (mm) | Calculated coordinate with bias correction by Method 2 (mm) |
|---|---|---|---|---|
| 1–1 | (−8,−26,28) | (−19.80,−29.70,39.12) | (−13.77,−20.87,27.73) | (−14.09,−21.13,27.83) |
| 1–2 | (−13,−25,57) | (−22.92,−40.46,63.43) | (−16.04,−28.64,45.11) | (−16.32,−28.82,45.18) |
| 2 | (−5,9,25) | (−11.10,15.38,27.77) | (−8.96,11.86,23.11) | (−9.18,12.71,22.96) |
| 3 | (−15,−23,31) | (−21.95,−29.77,57.65) | (−16.04,−21.06,41.57) | (−16.03,−21.57,42.11) |

Table 4
Euclidean distance (ED) between true and calculated coordinates of ROI in MRI cases

| Case no. | ED between true and calculated coordinate (without bias correction) (mm) | ED between true and calculated coordinate (with bias correction by Method 1) (mm) | ED between true and calculated coordinate (with bias correction by Method 2) (mm) |
|---|---|---|---|
| 1–1 | 16.63 | 7.73 | 7.8 |
| 1–2 | 19.46 | 12.81 | 12.86 |
| 2 | 9.25 | 5.24 | 5.95 |
| 3 | 28.36 | 10.79 | 11.23 |

*6.2.2. MR breast image experiments*

In order to further substantiate our 3D localization system in clinical trials, we used MR images to verify the system. Three patients showing microcalcifications on mammograms were also asked to take MR image at the same time. Four cases were collected (one patient had two groups of clustered microcalcifications) at the Tri-Service General Hospital. Since MR images were taken without compressing breasts, they provided the true coordinates of the cluster microcalcifications for validation of our systems. Table 3 tabulates true and calculated coordinates of the cluster microcalcifications in the four cases. Table 4 also tabulates the errors resulting from our proposed 3D localization system and Methods 1 and 2. Comparing Table 2 with Table 4, the results obtained by phantom and MR image experiments were very close, which justified the utility of the system in clinical applications.

### 6.3. Discussions

According to the results of experiment, we will further discuss the improvement to the presently method by using the proposed method in this paper, and also make a comparison with a method which was proposed by Kita et al. in 2002 [6].

*6.3.1. The improvement to the presently method*

Presently, radiologists generally rely on their experience to envision the relative positions of lesions in CC and MLO views prior to needle biopsy. In many cases, they also use the same way to help surgeons do wire localization to identify the lesions in their surgeries. The way that radiologists perform to envision the relative positions of lesions is exactly the same procedure described in Section 3 without any bias correction. Second columns of Tables 2 and 4 show that the Euclidean distance between true and calculated coordinates with no bias correction produced errors ranging from 4.6 to 36.97 mm with the average error of 19.8 mm. However, if the bias correction was included in the method proposed in this paper, such as Method 1, the results in third columns of Tables 2 and 4 showed the improvement with error reduced from 2.93 to 14.9 mm and average error decreased to 8.88 mm. It implies that with the bias correction method the localization accuracy could be significantly improved with error rate reduced to more than 55%. This also means that our proposed method can actually improve radiologists' 3D localization procedure which does not do bias correction.

*6.3.2. Comparison with Kita et al.'s method*

As mentioned in Section 1, the work on 3D localization for mammography has not received much interest and only a few papers were published in the literature. Kita et al.'s paper [6] is most representative among them. They proposed five steps of processes, A: back projection → B: uncompression → C: rotation → D: compression → E: projection to calculate the epipolar curve, that is the locus of possible corresponding positions of the point in the other image. Similarly, they also used MR breast images to validate their method. As concluded in their paper, they indicated that their system achieved errors within 10–20 mm in estimating the 3D locations of lesions which were close ours. However, their method is much more complicated than our proposed method. Such complexity may increase difficulty in design of a CAD system to realize their method and reduces its efficacy. Besides, Kita et al's method requires more information of input data than what our proposed method does. For example, Kita et al.'s method needs the information of angular separation between the CC and MLO directions, the thicknesses of the compressed breast in both CC and MLO views. Such required information is not part of process of taking mammograms and certainly overburdens radiologists. In addition, Kita et al. also needed to know the position of the same lesion in both views which is not required for our proposed system where only one view is sufficient.

## 7. Conclusion

Presently, radiologists must rely on their experience to envision the relative positions of lesions in CC and MLO views prior to needle biopsy. In some cases, they have to use needle localization to identify their exact locations. In this paper, the problem of how to reliably localize clustered microcalcifications in a 3D visualization space is addressed. In order to do so, the clustered microcalcifications in CC and MLO views must be registered first. This is done by extracting features from clustered microcalcifications that are independent of their spatial locations in both views. Finally, the registered clustered microcalcifications are represented by a 3D breast model and displayed in a 3D visualization space. Such a 3D localization takes advantage

of breast depth information provided by CC and MLO views which allows us to reliably locate positions of clustered microcalcifications in a 3D visualization space before surgical operation. Additionally, it also improves the efficiency of diagnosis for clustered microcalcifications of breast cancer and further reduces the waste of medical resource. Although the developed techniques are still in an early stage, our experiments have demonstrated its value in clinical applications.

## Acknowledgements

The work was supported by National Science Council and Taichung Veterans General Hospital, Taiwan under the grant NSC90-2213-E-006-092, TCVGH-895501C, respectively.

## References

[1] Niklason LT, Christian BT, Niklason LE, Kopans DB, Slanetz PJ, Castleberry DE, et al. Digital breast tomosynthesis: potentially a new method for breast cancer screening. Proceedings of the fourth international workshop digital mammography, Nijmegen, The Netherlands 1998 pp. 51–6.
[2] Maidment AD, Conant EF, Feig SA, Piccoli CW, Albert M. 3Dimension analysis of breast calcifications. Proceedings of the third international workshop digital mammography, Chicago, IL 1996 pp. 245–50.
[3] Chang Y-H, Good WF, Sumkin JH, Zheng B, Gur D. Computerized localization of breast lesion from two views an experimental comparison of two methods. Invest Radiol 1999;34(9):585–8.
[4] Cho BH, Woo JH, Mun WK, Kim IY. The localization and visualization of breast lesion in digitized mammogram. Proceedings of the 22th annual EMBS international conference, Chicago IL 2000 pp. 23–8.
[5] Yam M, Brady M, Highnam R, Behrenbruch C, English R, Kita Y. Three-dimensional reconstruction of microcalcification clusters from two mammographic views. IEEE Trans Med Imag 2001;20:479–89.
[6] Kita Y, Tohno E, Highnam RP, Brady M. A CAD system for the 3D location of lesions in mammograms. Med Image Anal 2002;6:267–73.
[7] Pal NR, Pal SK. Entropic thresholding. Signal Process 1989;16: 97–108.
[8] LO CS, Chung PC, Lee SK, Chang C-I, Lee T, Hsu GC, et al. Off-line mammography screening system embedded with hierarchically-coarse-to-fine techniques for the detection and segmentation of clustered microcalcifications. IEICE Trans Inf Syst 2000;E83D(12):2161–73.
[9] Cover T, Thomas J. Elements of information theory. New York: Wiley; 1991.
[10] Chandrasekhar R, Attikiouzel Y. A simple method for automatically locating the nipple on mammograms. IEEE Trans Med Imag 1997; 16(5):483–94.

**Sheng-Chih Yang** received his BS degree in Electronic Engineering from National Chin-Yi Institute of Technology, Taiwan in 1987 and his MS degree in Computer and Information Science from Knowledge System Institute, IL, USA in 1996. From 1992 to 1996, he worked as a Teaching Assistant at the Department of Electronic Engineering, National Chin-Yi Institute of Technology, and has been a Lecturer since 1996. He is currently a PhD candidate in the Department of Electrical Engineering, National Cheng-Kung University, Taiwan. His research interests include image processing and biomedical image processing.

**Hsian-He Hsu** received his MD degree from National Defense Medical Center, Taiwan, in 1989. He is currently an attending Radiologist at Tri-Service General Hospital, National Defense Medical Center, Taiwan, Republic of China. His research interests include X-ray mammograms, ultrasound screening of breast cancer, computed tomography, and magnetic resonance imaging.

**Giu-Cheng Hsu** received his MD degree from National Defense Medical Center, Taiwan, in 1984. From 1985 to 1989 he serviced at Tri-Service General Hospital from resident to staff of Diagnostic Radiology. In 1990, he received a year of clinical fellowship training in Iris Cantor Breast Imaging Center at UCLA. Since then he has participated in breast imaging study in Taiwan Adventist Hospital and Tri-Service General Hospital. He is currently the Chief of Women's Health Center at Tri-Service General Hospital. His research interests include mammography and ultrasound screening of breast cancer, picture archiving and communicating system, and computed aided diagnosis (CAD) in X-ray mammograms.

**Pau-Choo Chung** received the BS and MS degrees in electrical engineering from National Cheng Kung University, Taiwan, Republic of China, in 1981 and 1983, respectively, and the PhD degree in electrical engineering from Texas Tech University in 1991. In 1991, she joined the Department of Electrical Engineering, National Cheng Kung University, and has become a full professor since 1996. Currently, she also serves as the vice director of the Center for Research of E-life Digital Technology, National Cheng Kung University. Dr Chung's research interests include image analysis and pattern recognition, computer vision, video image processing/analysis, neural networks, telemedicine, and multimedia transmission. Particularly she applies most of her research results on medical applications, such as for medical image analysis, broadband telemedicine, pervasive home care, and multimedia-based behavior analysis. She received many awards, such as the annual best paper award in Chinese Journal Radiology 2001, the best paper awards from World Multiconference on Systemics, Cybernetics, and Informatics (SCI) 2001 and International Computer Symposium (ICS) 1998, Acer's Best Research Award in 1994 and 1995, the best paper awards from the Conference of Computer Vision, Graphics, and Image Processing (CVGIP), in 1993, 1996, 1997, 1999, and 2001, Best Research Young Innovator Award (NSC) 1999. Dr Chung has served as the program committee member in many international conferences. She is a senior member of IEEE and Member of Phi Tau Phi honor society. Currently she is also serving as the associate editor of Journal of Information Science and Engineering, the Chair of IEEE Computational Intelligence Society Tainan Section, the Newsletter Editor of IEEE Tainan Section, and the secretary of Biomedical Engineering Society. She is also one of the founders of DICOM Association in Taiwan.

**Shu-Mei Guo** received MS degree in Department of Computer and Information Science from New Jersey Institute of Technology, USA in 1987. She received the PhD degree in Computer and Systems Engineering from University of Houston, USA in 2000. Since 2000, she has been an assistant professor in Department of Computer System and Information Engineering, National Cheng-Kung University, Taiwan. Her research interests include various applications on evolutionary programming, chaos systems, Kalman filtering, fuzzy methodology, sampled-data systems, image processing, and computer and systems engineering.

**Chien-Shun Lo** received the BS and MS degree in Information Engineering and Computer Science from Feng-Chia University, Taiwan, ROC, in 1992 and 1994, respectively, and the PhD degree in electrical engineering from National Cheng-Kung University, Taiwan, ROC, in 2000. From 2000 to 2004, he was with Newsoft Technology Corporation working on the development of multimedia and MPEG technology. Since October 2004, he has been with Department of Multimedia Design, National Formosa University, where he is currently an Assistant Professor. His current research includes computer aided diagnostic system design, medical image processing, video processing, and streaming technology.

**Ching-Wen Yang** received the BS degree in information engineering sciences from Feng-Chia University, Taiwan, Republic of China, in 1987, the MS degree in information engineering from National Cheng Kung University in 1989, and the PhD Degree in electrical engineering from National Cheng Kung University, Taiwan, Republic of China, in 1996. He is currently a chief in the Computer and Communication Center at Taichung Veterans General Hospital, Taiwan. His research interests include image processing, biomedical image processing and computer networks.

**San-Kan Lee** received his MD degree from National Defense Medical Center, Taiwan, in 1973. From 1976 to 1989 he serviced at Tri-Service General Hospital from resident, visiting staff, and eventually as Director of Division of Diagnostic Ultrasound. In 1982, he received a year of clinical fellowship training at Division of Diagnostic Ultrasound of Thomas Jefferson University Hospital in Philadelphia. From 1990 to 2003, he was Chairman of Department of Radiology at Taichung Veterans General Hospital. His current position is the President of Suao Veterans Hospital in Yilan County, Taiwan. He is a Professor of Radiology of National Defense Medical Center and Chung Shan Medical University. His research interest includes computed aided diagnosis (CAD) in X-ray mammograms, ultrasound screening of breast cancer, picture archiving and communicating system, and computed tomograph. Dr Lee has published over 200 peer-reviewed papers, and presented more than 50 abstracted in the international conferences. He also has one US and one Taiwan patents.

**Chein-I Chang** received his BS degree from Soochow University, Taipei, Taiwan, 1973, MS degree from the Institute of Mathematics at National Tsing Hua University, Hsinchu, Taiwan, 1975 and MA degree from the State University of New York at Stony Brook, in 1977, all in mathematics. He also received his MS, MSEE degrees from the University of Illinois at Urbana-Champaign, in 1982 and PhD degree in electrical engineering from the University of Maryland, College Park, in 1987. Dr Chang has been with the University of Maryland Baltimore County (UMBC) since 1987, as a visiting assistant professor from January 1987 to August 1987, Assistant Professor from 1987 to 1993, associate professor from 1993 to 2001 and professor in the Department of Computer Science and Electrical Engineering since 2001. He was a visiting research specialist in the Institute of Information Engineering at the National Cheng Kung University, Taiwan, from 1994 to 1995. He received an NRC (National Research Council) senior research associate ship award from 2002 to 2003 sponsored by the US Army Soldier and Biological Chemical Command, Edgewood Chemical and Biological Center, Aberdeen Proving Ground, Maryland. He has three patents and several patents pending. He is on the editorial board of the *Journal of High Speed Networks* and was the guest editor of a special issue of the same journal on telemedicine and applications. His research interests include multispectral/hyperspectral image processing, automatic target recognition, medical imaging, information theory and coding, signal detection and estimation and neural networks. He has authored a book, Hyperspectral Imaging: Techniques for Spectral Detection and Classification published by Kluwer Academic Publishers. Dr Chang is an Associate Editor in the area of hyperspectral signal processing for IEEE Transaction on Geoscience and Remote Sensing and a Fellow of SPIE and a member of Phi Kappa Phi and Eta Kappa Nu.